Atmospheric Research 163 (2015) 146–161

Contents lists available at ScienceDirect

Atmospheric Research

journal homepage: www.elsevier.com/locate/atmos

Evaluation of high-resolution satellite precipitation estimates over southern South America using a dense rain gauge network

Paola Salio [a,b,c,*], María Paula Hobouchian [d], Yanina García Skabar [c,d,e], Daniel Vila [f]

[a] Centro de Investigaciones del Mar y la Atmósfera, CONICET-UBA, Buenos Aires, Argentina
[b] Departamento de Ciencias de la Atmósfera y los Océanos, FCEN-UBA, Buenos Aires, Argentina
[c] Instituto Franco-Argentino sobre Estudios de Clima y sus Impactos UMI 3351 CNRS–CONICET–UBA, Argentina
[d] Servicio Meteorológico Nacional, Buenos Aires, Argentina
[e] Consejo Nacional de Investigaciones Científicas y Técnicas, Argentina
[f] Divisão de Satélites e Sistemas Ambientais, CPTEC-INPE, Brazil

ARTICLE INFO

Article history:
Received 10 March 2014
Received in revised form 20 November 2014
Accepted 21 November 2014
Available online 28 November 2014

Keywords:
Multisensor quantitative precipitacion estimates
Precipitation
Validation
South America

ABSTRACT

Six different satellite rainfall estimates are evaluated for a 24-hour accumulation period at 12 UTC with a 0.25 degree resolution. The rain gauge data are obtained from a dense inter-institutional station network for December 1, 2008 to November 30, 2010 over South America. The evaluated satellite rainfall products are the Tropical Rainfall Measuring Mission 3B42 V6, V7 and RT, the NOAA/Climate Prediction Center Morphing technique (CMORPH), Hydroestimator (HYDRO) and the Combined Scheme algorithm (CoSch). The validation and intercomparison of these products are focused on southern South America. The performance improves in the "blended" estimates by including microwave observations and surface observations in the adjustments, i.e., 3B42 V6, V7 and CoSch; however, large overestimations are detectable in CMORPH, principally for extreme values over plains areas. The estimates based on parameters associated with infrared images only (HYDRO) underestimate precipitation south of 20° S and tend to overestimate the warm precipitation to the north. The inclusion of observed precipitation data is convenient from monthly (3B42 V7 and V6) to daily scales (CoSch) and improves the estimates. The estimates that include microwave observations show a strong tendency to overestimate extreme values of precipitation over 70 mm. This effect is strongly evident in northern and central Argentina and southern Brazil. A deeper assessment is necessary, particularly over the Central Andes, where effects of topography principally associated with solid precipitation correspond to the persistence of majorly overestimated precipitation.

1. Introduction

Precipitation plays a fundamental role in regulating the climate system. The knowledge of the areas where precipitation occurs enables management of water resources, the prevention of natural disasters and, consequently, better developed human activities. For this reason, accurate precipitation measurements provide important information for decision making by multiple users (Kucera et al., 2013).

Precipitation measurement is a major challenge due to the high spatial and temporal variability. The knowledge of the structure of precipitation requires observing networks with very high spatial and temporal resolutions, which are difficult to implement in areas covered by deserts, mountains, and oceans and in large areas with low population densities. This issue also presents a challenge for developing countries in South America where the maintenance of these networks is extremely expensive.

Rain gauges are the principal source of direct precipitation measurements in South America and are necessary for calibrating and validating precipitation estimates obtained from indirect measurements – radar or satellite – and numerical models. However, observations over South America are insufficient and unevenly distributed. Their temporal resolution is low, i.e., the accumulation periods are 24 hours or, occasionally, 6 hours.

The introduction of meteorological satellites in the 1970s made it possible to perform hemispheric observations of cloudiness. This encouraged scientific research on multiple satellite-based remote sensing technique of meteorological variables. However, estimates of precipitation based on radiometric observations are an ongoing challenge. The first techniques used visible (VI) and infrared (IR) wavelength data to infer precipitation based on cloud reflectivity and cloud top temperature, respectively (Arkin and Meisner, 1987; Scofield and Kuligowski, 2003 and all of the papers cited therein). Non-precipitating clouds with cold tops can be easily misinterpreted as highly precipitating systems if IR data are used. However,

* Corresponding author at: CIMA-CONICET-UBA/DCAO UBA-FCEN/UMI3351-CNRS-CONICET-UBA Intendente Güiraldes 2160 - Pabellon 2 - 2° Piso Ciudad Universitaria C1428EGA - Buenos Aires – Argentina.
E-mail address: salio@cima.fcen.uba.ar (P. Salio).

http://dx.doi.org/10.1016/j.atmosres.2014.11.017
0169-8095/

precipitation is not necessarily associated with cold clouds; in some cases, precipitation develops from warm and relatively low clouds as observed in the development stage of deep convection and in tropical areas (Houze, 1994).

Introducing passive microwave (PM) measurements on satellite platforms made it possible to develop algorithms that explain the internal structure of cloudiness based on the analysis of the attenuation of the PM field generated by cloudiness. These algorithms generally provide more accurate estimates of instantaneous precipitation than the algorithms based on VI or IR data on the global scale (Ebert et al., 1996; Smith et al., 1998; Ebert et al., 2007). However, the advantage of using IR equipment onboard geostationary satellites to generate precipitation estimates is the finer spatial and temporal resolutions and nearly global coverage compared to the PM observations of polar-orbiting satellites where only one image is retrieved every three hours from a large range of orbits of different satellites.

Precipitation products derived from combining IR observations (higher spatial and temporal resolution) with PM observations (high quality), known as "blended techniques," perform better in the global context (Ebert et al., 2007). A large number of IR-PM algorithms was developed using different strategies to optimally include both estimates (Huffman et al., 2001; Xu et al., 1999; Miller et al., 2001; Kidd et al., 2003; Sorooshian et al., 2000; Kuligowski, 2002; Joyce et al., 2004) and to consider surface information in the calibration procedure (Huffman et al., 2007; Vila et al., 2009; Kidd and Levizzani, 2011). An updated list of the available estimations is presented in Table 2 in Tapiador et al. (2012).

The performances of products over South America have recently been assessed and present several challenges. South America, a region that experiences some of the most intense mesoscale convective systems (MCSs) on Earth (Zipser et al., 2006), has areas of complex topography (i.e., the Andes cordillera), snow-covered surfaces, and heavy precipitation from warm clouds in areas such as northeastern Brazil and the Amazon (Liu and Zipser, 2009). Su et al. (2008) validated the daily TRMM Multi-satellite Precipitation Analysis (3B42; Huffman et al., 2007) version 6 for La Plata Basin and found that it performed well on the monthly scale and that performance decreased on the daily scale, mainly at the highest precipitation thresholds. In addition, results of inputting 3B42 V6 data into hydrological models show the ability of the method to capture flood-related events and the seasonal and interannual variability of river streamflow; thus, it is a potential tool for hydrological forecasting in the region. When verifying this method on the daily scale, Ruiz (2009) found that although the CPC MORPHing Technique (CMORPH; Joyce et al., 2004) captures precipitation events adequately and despite the good relationship in the relative intensity of each of those events, the technique tends to overestimate mean precipitation over eastern Argentina, Uruguay and in the area close to the border of Paraguay in Brazil. Vila et al. (2009) and Rozante et al. (2010) assessed the performance of the Combined Scheme (CoSch; Vila et al., 2009) for summer and winter estimates over South America; De Vera and Terra (2012) applied a similar methodology for Central Uruguay. The results showed that over areas with a high density of rain gauge observations, this technique is equivalent to averaging rain gauge data over the available grid points, while in areas where the observation network is coarser, the results are better and indicate the potential of this product. Dinku et al. (2010a, 2010b) validated seven satellite precipitation estimates on daily and 10-day time scales in an area of complex topography in Colombia. The best results were obtained for the plains area in eastern Colombia, and the product performance was markedly worse on the Pacific Coast. In this case, CMORPH performed well compared with the other analyzed products.

The previously described examples show that progress is needed to determine the quality of these products for South America and to provide an adequate evaluation for different users. The studies mentioned explore individual estimates for an area of interest, but a thorough study assessing the performance of multiple estimates using high spatial density rain gauge networks is lacking over these areas. This study focuses on assessing the performance of satellite rainfall estimates available over the area, particularly southern South America, by validating the data using available 24-hour information over a dense rain gauge network. The data and methodology are described in Section 2. The results of the product intercomparison are presented in Section 3. Lastly, the discussion and conclusions are provided in Section 4.

2. Data and methodology

2.1. Rain gauge information

The present study was conducted over a period of 2 years, from December 1, 2008 to November 30, 2010. The period was selected based on the availability of rain gauge information. An extensive rain gauge network that covers Argentina, Bolivia, Brazil, Chile, Paraguay, and Uruguay was used in this study. Fig. 1 shows the number of rain gauges available in 0.25° latitude by 0.25° longitude boxes. A total of 5414 stations are available during the selected period. Data were interpolated to a 0.25° resolution grid by averaging the available data over each 0.25° × 0.25° area and assigning the mean value to the center of the grid. This methodology had been applied by Liebmann and Allured (2005). The methods used to grid the observations for matching rain gauge and satellite data have several problems, and many studies show that there is no single algorithm outperformance in all conditions (Ebert et al., 2007; Porcu et al., 2014). In areas with not equally distributed and sparse rain gauges, the different rain gauge analysis will provide similar results. In this case, data were interpolated to a 0.25° resolution grid by averaging the available data over each 0.25° × 0.25° area and assigning the mean value to the center of the grid. This methodology had been applied by Liebmann and Allured (2005), who obtained good results for the region. In the same way, DeMaria et al. (2011) indicated that the impact of the interpolation method does not have an effect on the results of a similar study over southeastern South America. The available network is unevenly distributed over 3881 grid points. To achieve the most representative and consistent data for verification, only grid points that have information for at least 70% of the days were taken into account.

It is important to emphasize that the observation network used in this study is composed of numerous networks that are not available in real time to any of the institutions in charge of adjusting precipitation estimates; thus, this database is the subject of a major assessment. In turn, for a correct validation, data retrieved from the Global Telecommunication System were excluded from the data set. This study considers 24-hour accumulated precipitation at 12 UTC.

Data were provided by the following institutions: Dirección General de Aguas — Chile, Servicio Meteorológico Nacional — Argentina; Administración Provincial del Agua — Chaco, Argentina; Subsecretaría de Recursos Hídricos de la Nación — Argentina; Universidad de La Punta — San Luis, Argentina; Autoridad Interjurisdiccional del Agua — Neuquén, Argentina; Instituto Nacional de Tecnología Agropecuaria — Argentina; Bolsa de Cereales — Argentina; Dirección Nacional de Meteorología — Uruguay; Dirección de Meteorología e Hidrología — Dirección Nacional de Aeronáutica Civil — Paraguay; Comisión Técnica Mixta Salto Grande; Centro de Previsão de Tempo e Estudos Climáticos — Brazil; National Oceanic and Atmospheric Administration — USA.

At the database development stage, a thorough quality control was performed on the observations; it mainly consisted of analyses of extremes, contiguous values and days without precipitation.

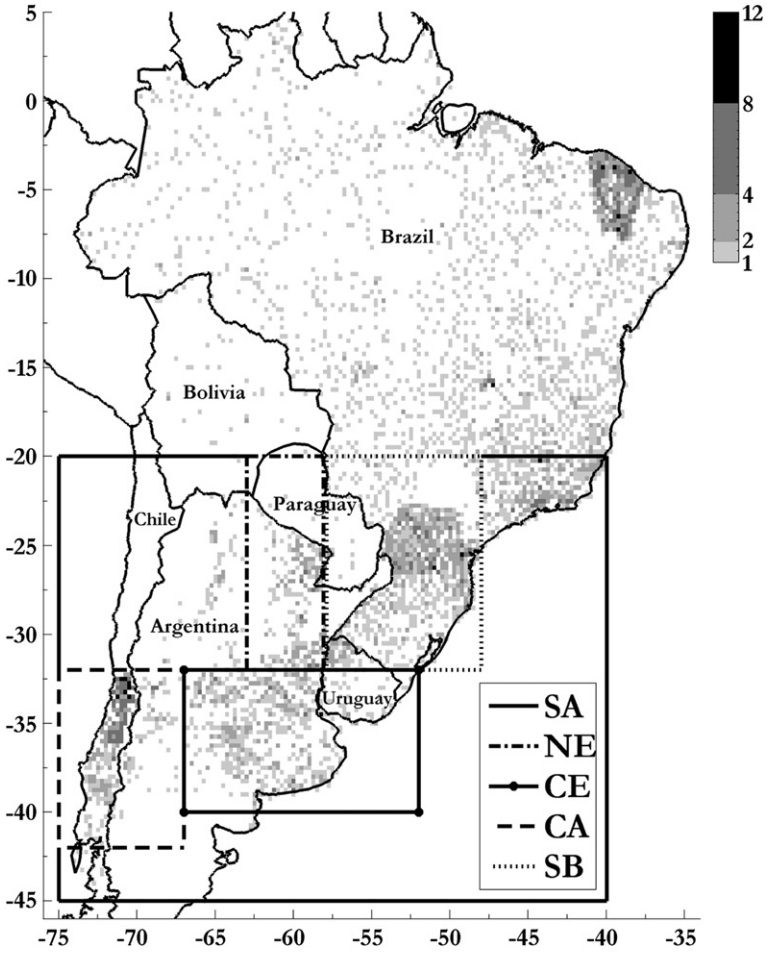

Fig. 1. Available observational network interpolated to a 25 km resolution grid over South America; gray areas indicate that more than 70% of the information is available in the selected period. Shading denotes the number of stations available in the 0.25 degree grid box. Countries and geographical areas mentioned in the text are also shown. The regions considered are southern South America (SA), northeastern Argentina (NE), Central Argentina and Uruguay (CE), Central Andes (CA), and southern Brazil (SB).

Extreme events were analyzed on a case-by-case basis to identify incorrect data. Days with no precipitation records in the observed or estimated grids were not considered in the sample.

2.2. Precipitation estimates

Four of the available satellite-derived precipitation estimates products using microwave fields were analyzed in this study: CMORPH, 3B42 in its operational version RT, and versions 6 (3B42 V6) and 7 (3B42 V7). All estimations have 0.25° spatial resolutions and 3-hour temporal resolutions. There are methodological differences among the mentioned algorithms. CMORPH uses infrared measurements from geostationary satellites to estimate the motion of cloud systems, while 3B42 RT compares IR and microwave fields and adjusts the accumulated precipitation field. The 3B42 V6 algorithm combines all available microwave estimates through the "histogram matching" technique, converts the brightness temperature of the infrared channel into precipitation rates based on calibrated microwave data, and obtains calibration curves from monthly observed precipitation data to recalculate 3-hourly accumulated data on the grid to obtain instantaneous precipitation rates. Improvements were introduced to the 3B42 V7 algorithm, specifically, the consideration of microwave moisture soundings and uniformly reprocessed input data (Huffman and Bolvin, 2013). The consideration of the 3B42RT algorithm is essential due to its important role for operational activities in the region. The Combined Scheme (CoSch) following the technique proposed by Vila et al. (2009) is also used in the intercomparison of 24-hour accumulated data at 12UTC. CoSch adjusts 3B42 RT data with ground observations available through the Global Telecommunication System and other regional networks with 24-hour accumulated data using a technique to remove the bias between observed and estimated data. Hydroestimator (HYDRO; Vila et al., 2002; Scofield and Kuligowski, 2003) is one of the estimates based on brightness temperature from 4th channel retrieved from geostationary orbit satellites and correction factors from numerical model information. Due to the rapid updates of IR information from geostationary satellites, including values valid at operating times, HYDRO is widely used in the region. The version used in this study is available from the Centro de Previsão de Tempo e Estudos Climáticos — Brazil; the data are available every 30 minutes with a spatial resolution 4 km. The most recent version of this algorithm over South America uses the CPTEC/ETA Regional Model output to improve the performance of this technique; precipitable water between the surface and 500 hPa is used for adjusting the power-law relation between cloud-top temperature and precipitation rates, while surface relative humidity is applied for adjusting the final rain rates. These adjustments decrease rainfall rates in very dry environments and increase them in very moist environments. Low-level winds and a digital elevation model are also used for improving rainfall over complex terrain (Vila et al., 2002; Vicente et al., 2001).

Taking into account the spatial resolutions of the different estimates and the rain-gauge network available for the present work, a

resolution of 0.25° is used for all estimates. This resolution is detrimental to some estimates with higher resolutions, but most of the areas have only one station in the 0.25° grid box (Fig. 1) and a validation with higher resolution is not suitable.

2.3. Intercomparison methodology

The validation of satellite-derived precipitation estimates was mainly focused on the subtropical region of South America, which encompasses a wide range of precipitation regimes. Therefore, to take into account the different regimes within the region, the domain was divided into homogeneous areas in terms of density of observations and climate conditions (Fig. 1). Moreover, the differences that arise between warm and cold seasons must also be considered. During winter, the precipitation over large areas of subtropical South America is associated with the passage of weather systems, while the summer precipitation maintains a convective nature. A more suitable verification can be achieved by dividing the domain into seasons and regions according to their climate regimes.

The analysis considers a vast area in South America south of 20° S (SA) and four subregions within SA with different characteristics in terms of the amount, intensity and duration of precipitation: northeastern Argentina (NE), southeastern Brazil (SB), central-eastern Argentina and Uruguay (CE), and the complex topographical region of the Central Andes (CA). A humid subtropical climate dominates in NE and SB and is characterized by warm and rainy summers and winters with frequent intrusions of polar fronts and the passage of weather systems. The area is divided into two sections, given that precipitation data are much denser in SB. Fig. 2 shows the annual 24-hour accumulated precipitation in which SB exhibits a peak that does not extend to NE. The region called CE has a humid subtropical climate in the east and a mid-latitude dry continental climate in the west; tropical continental air is present in summer and polar continental air is present in winter. The peak precipitation south of the Central Andes (CA) mainly occurs in winter. A more complete description of the climate and precipitation regimes of each region is provided by Strahler (1969) and Schwerdtfeger (1976).

The verification was performed annually and seasonally using the root mean square error, which provides a measure of the mean value of estimate errors; the bias represents the systematic error of the estimates. Both statistics were normalized by the daily precipitation rate of the analyzed period to achieve comparable values for different seasons and regions following the methodology used by Su et al. (2008). The normalized root mean square error (NRMSE), the percent bias (BIAS%) and the correlation coefficient (CORR) are defined as follows:

$$\mathrm{NRMSE} = \sqrt{\frac{\sum_{i=1}^{N}(P_e - P_o)^2}{\frac{N}{\sum_{i=1}^{N} P_o}{N}}} \tag{1}$$

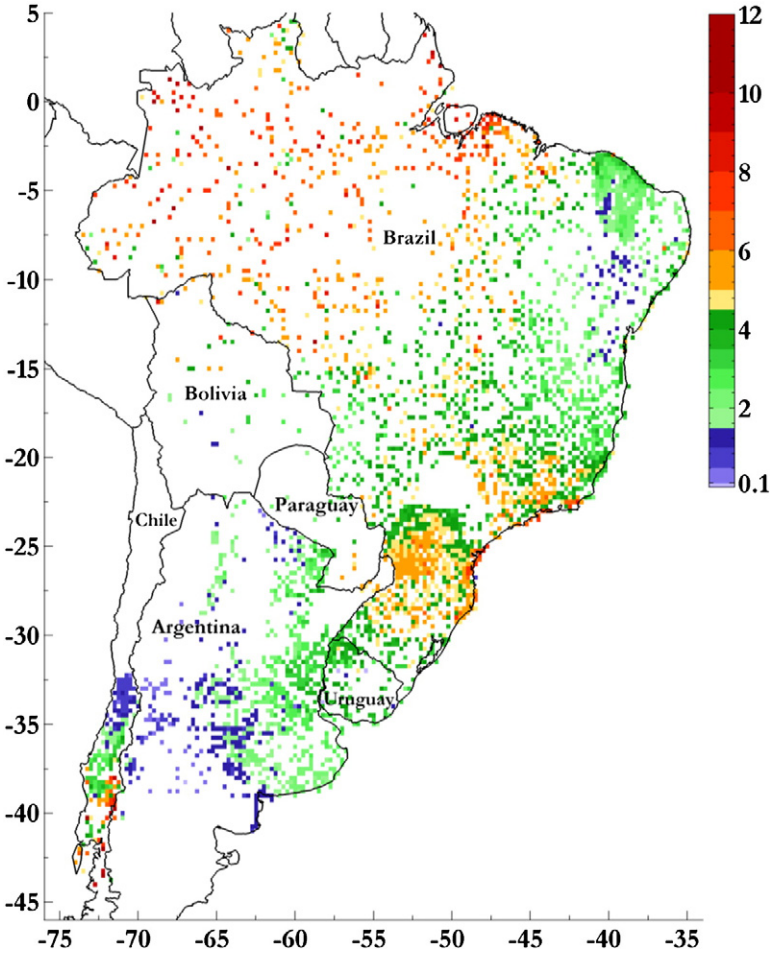

Fig. 2. Mean 24-hour accumulated precipitation (mm) from the available observational network over South America.

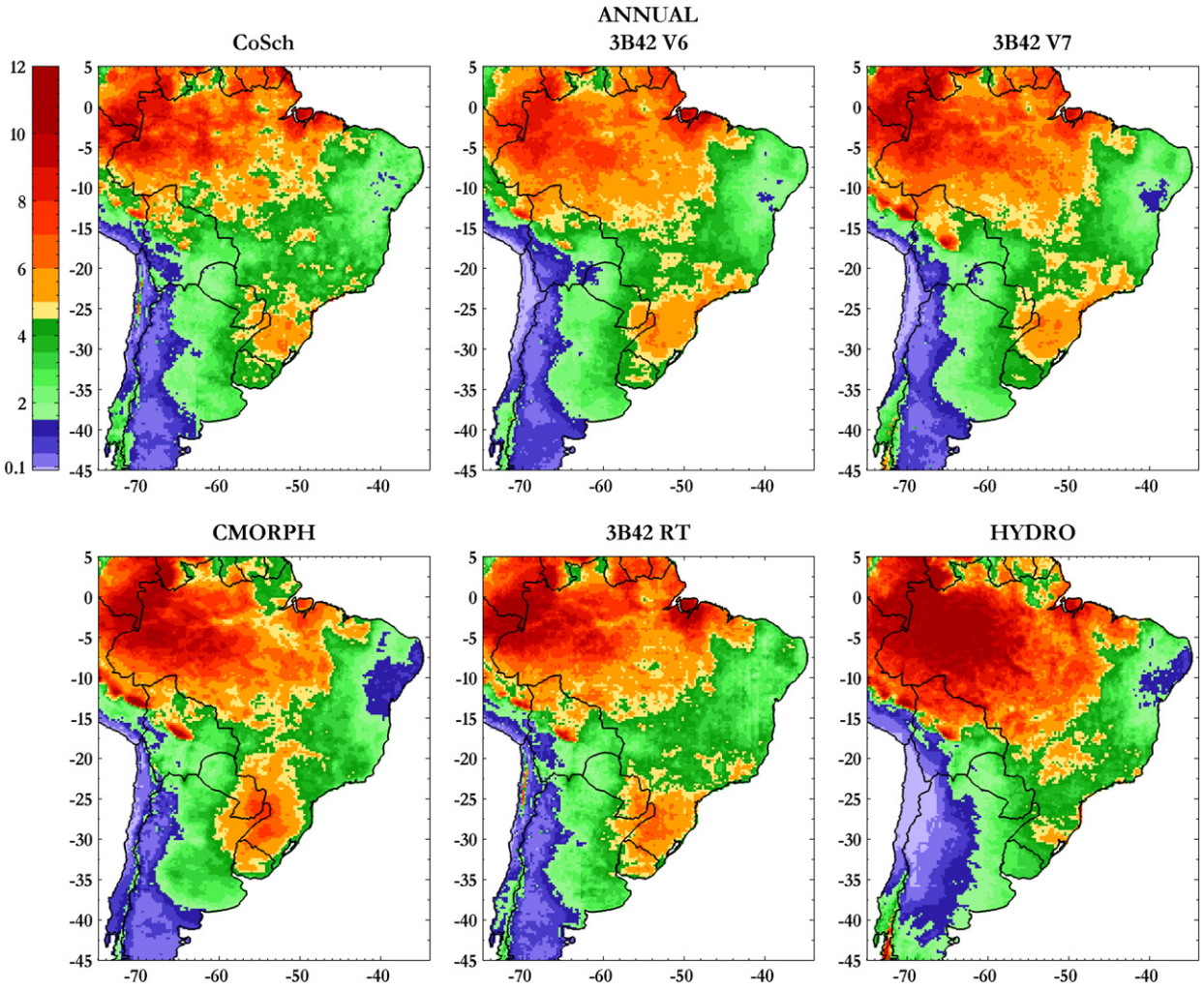

Fig. 3. Mean 24-hour accumulated precipitation (mm) in the study period of the different precipitation estimations considered in the present study. Ocean areas were masked.

$$\mathrm{BIAS}\% = \frac{\sum_{i=1}^{N}(P_e - P_o)}{\sum_{i=1}^{N} P_o} \times 100 \tag{2}$$

$$\mathrm{CORR} = \frac{\sum_{i=1}^{N}(P_e - \overline{P}_e)(P_o - \overline{P}_o)}{\sqrt{\sum_{i=1}^{N}(P_e - \overline{P}_e)^2}\sqrt{\sum_{i=1}^{N}(P_o - \overline{P}_o)^2}} \tag{3}$$

where P_e and P_o are the estimated and observed precipitation, respectively, and N is the sum of grid points that were considered in the analysis of the corresponding period. The overline indicates the sample mean.

Categorical statistics, such as bias score (BIASS), equitable threat score (ETS), probability of detection (POD) and false alarms (FAR) are used for determining the quality of the estimates at the different precipitation intervals. These statistics are defined as follows:

$$\mathrm{BIASS} = \frac{H + F}{H + M} \tag{4}$$

$$\mathrm{ETS} = \frac{H - \frac{(H+M)(H+F)}{N}}{H + M + F - \frac{(H+M)(H+F)}{N}} \tag{5}$$

$$\mathrm{POD} = \frac{H}{H + M} \tag{6}$$

$$\mathrm{FAR} = \frac{F}{H + F} \tag{7}$$

where a hit (H) corresponds to a precipitation value observed and estimated above a threshold, a miss (M) corresponds to precipitation observed above a threshold but estimated below and a false alarm (F) corresponds to precipitation estimated above a threshold but observed below. BIASS measures the relationship between frequencies of an estimated event regarding frequencies of an observed event, the perfect value is 1. POD describes how many events were estimated correctly, the perfect value is 1. FAR complements the POD as it measures what fraction of an estimated events did not actually occur, perfect value is 0. ETS measures the fraction of observed and/or estimated events that were correctly predicted considering different thresholds. Multiple precipitation thresholds have been considered to calculate the statistics: 0.5, 1, 2, 3, 4, 5, 6, 7, 8, 9, 10, 12, 15, 20, 30 and 50 mm.

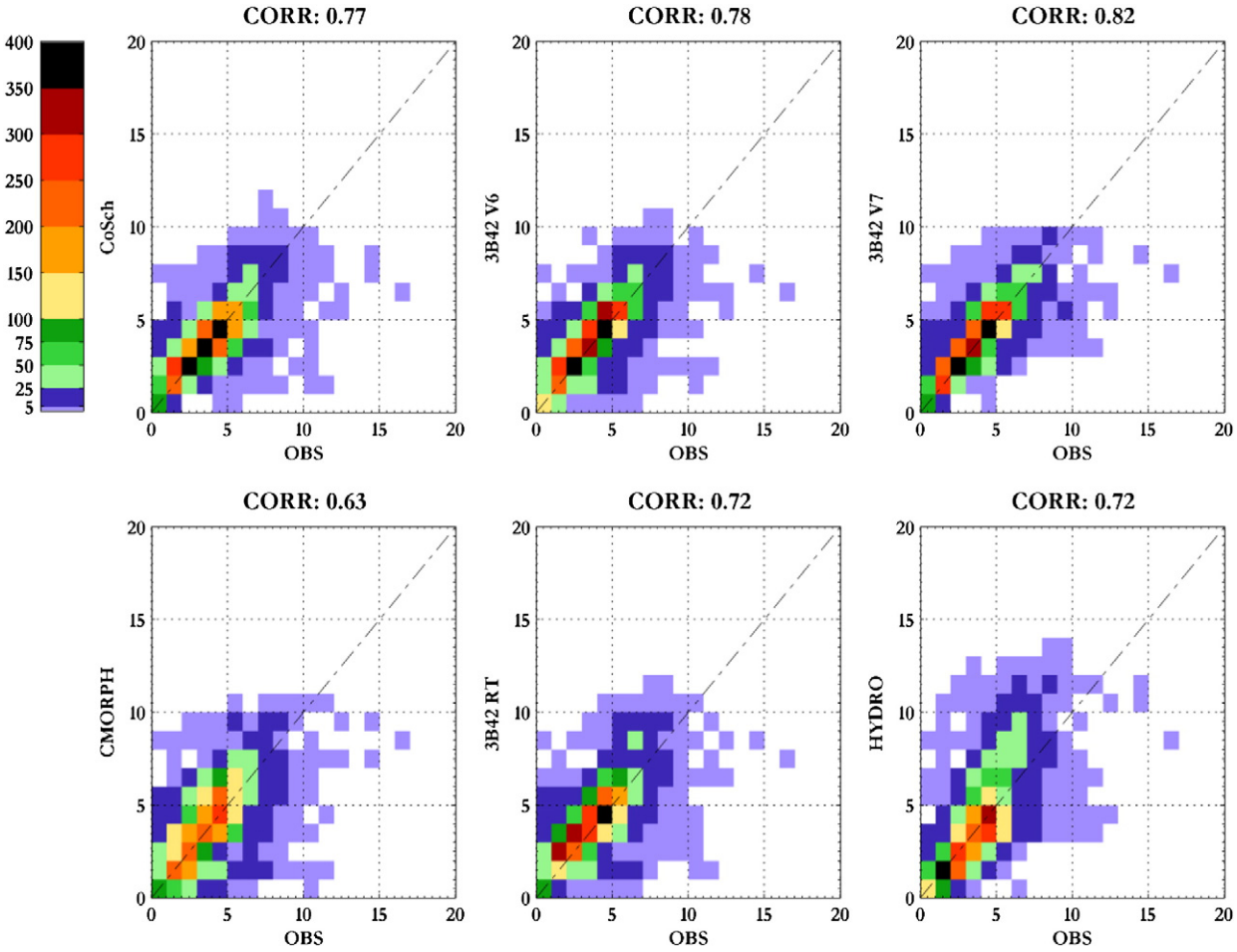

Fig. 4. Absolute frequency of events is showed in a two-dimensional histograms of 24-hour accumulated precipitation of observations vs. precipitation estimates over the whole grid in South America.

The statistics were analyzed within the areas previously described for the entire period under study. Box plots for those statistics were also plotted to assess similarities between the distributions of estimates and observations in terms of symmetry and dispersion for the purpose of determining the existence of extreme values (Ebert et al., 2007; Sapiano and Arkin, 2009).

In addition, the probability distribution of precipitation volumes (PDF, Amitai et al., 2012) was calculated for the different regions. PDF (Eq. (8)) considers the relative contribution of each precipitation interval to the total precipitation volume.

$$\mathrm{PDF}(R_i) = \frac{\int_{R_i-05}^{R_i+0.5} R\ P(R)\ \mathrm{d}R}{\int_{0}^{\infty} R\ P(R)\ \mathrm{d}R} \tag{8}$$

where R represents the amount of rainfall in mm and P is the rainfall detection probability. These PDFs have the advantage of being less sensitive to limitations in detecting weak precipitation (associated with a small fraction of the total precipitation) compared with PDFs of occurrence and are good for comparing surface observations with estimates derived from algorithms and instruments with different detection limits.

3. Results

3.1. Spatial analysis

To perform a preliminary qualitative analysis and identify the regions with maximum and minimum precipitation in South America, Fig. 3 presents the mean 24-hour accumulated precipitation calculated by the different estimates.

Based on a comparison with Fig. 2, the estimates are able to identify the regions of maximum and minimum observed precipitation. Two peak areas with daily rates above 6 mm/day are observed near the equator and in southeastern Brazil. All data overestimate the peak in the equatorial region. Estimates that are not corrected by observations present greater overestimations. The peak in Southeast Brazil is also overestimated, except that of HYDRO, which underestimates the precipitation rate over that region and over central-eastern Argentina. A smaller peak is observed over the Andes between 38° and 42° S. None of the estimates represents this peak; HYDRO is the only estimate that represents the peak, but it is weak.

The two-dimensional histograms displayed in Fig. 4 better depict the different estimates over the whole domain. CoSch, 3B42 V6 and 7 are clustered more closely about the 1:1 line, which is evident in the high correlation coefficient obtained by these estimates. HYDRO shows a strong tendency to overestimate values higher than 4 mm; this tendency is also present in 3B42 RT, but the signal is lower. All estimations show a tendency to overestimate small values.

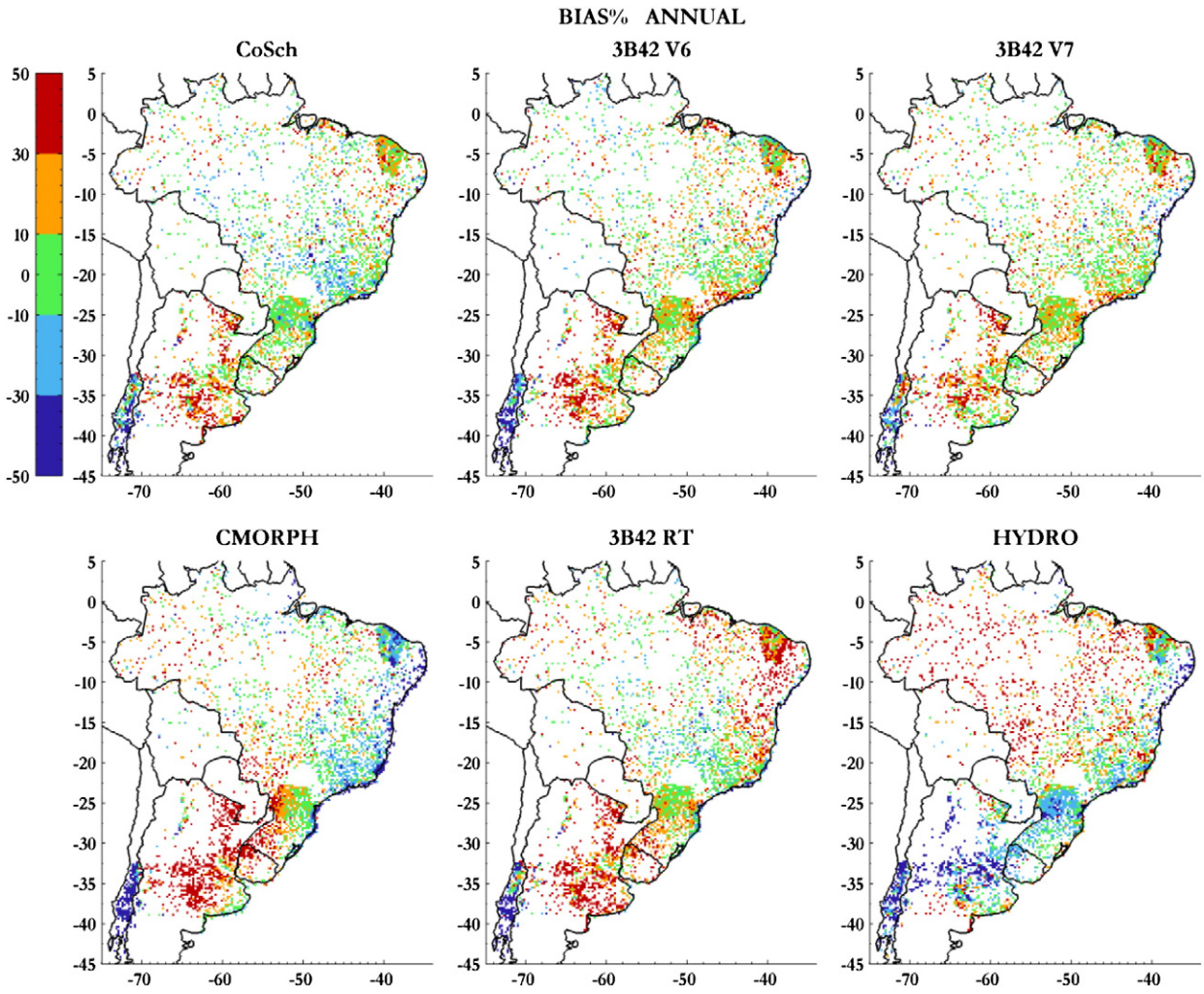

Fig. 5. BIAS% calculated for the study period of the different precipitation estimations considered in the present study.

To perform a quantitative spatial analysis of the deviations over the entire study region, spatial BIAS% maps were plotted (Fig. 5). For these fields, the BIAS% was calculated at the grid points with observations. The greatest biases appear in central and northern Argentina, where all of the estimates overestimate precipitation with BIAS% values above 50%. HYDRO presents completely opposite behavior and underestimates the precipitation of the whole region south of 20° S.

In general, CoSch performs better; the behaviors of 3B42 RT, V6 and V7 are similar, with greater BIAS% in those areas where CoSch fails. Versions 6 and 7 are able to improve the operational estimate using monthly precipitation observations calibrations. CoSch, considering a daily calibration, was able to improve a major overestimation that 3B42 RT maintains in southeastern Brazil. CMORPH presents the greatest positive BIAS% values over central and northeastern Argentina and indicates that precipitation is largely overestimated, which is also seen in northern and northwestern Brazil. In southeastern Brazil, the result is opposite, i.e., underestimations are produced. Lastly, HYDRO behaves differently to the south and north of the band between 25° S and 20° S; major precipitation underestimates occur in the subtropical area and positive BIAS% occurs over nearly the entire tropical region, except southeastern and eastern Brazil where the estimates remain below the observed precipitation. Unfortunately, the area associated with the maximum occurrence of large MCS (Salio et al., 2007; Zipser et al., 2006; Liu and Zipser, 2009) is centered at approximately 28° S–58° W, where the observation network density is low. However, there is a tendency of overestimation by all of the estimates, except HYDRO, where underestimation becomes evident in the surrounding area.

At the grid points located in the Central Andes region, all of the estimates show negative BIAS% over the windward mountain slopes; HYDRO, Cosch and 3B42 V7 perform better. These results are similar to those obtained by Ebert et al. (2007) and Gochis et al. (2009) for the Rocky Mountains. In any case, one has to consider that in complex mountainous areas, precipitation estimate errors may be related to the evaporation of precipitation before it reaches the surface and to errors associated with the difficulty of microwave algorithms in estimating precipitation over surfaces covered by snow (Ebert et al., 2007).

The precipitation regime in this area is extremely different between summer and winter; for this reason, Figs. 6 and 7 show the BIAS% in CA for austral summer and winter, respectively. Fig. 2 shows that the precipitation peak over this area occurs at approximately 40° S–72° W. The peak corresponds to winter, and it extends northward during this season; however, when the peak is near 35° S, the annual accumulated precipitation is below 100 mm and is mainly

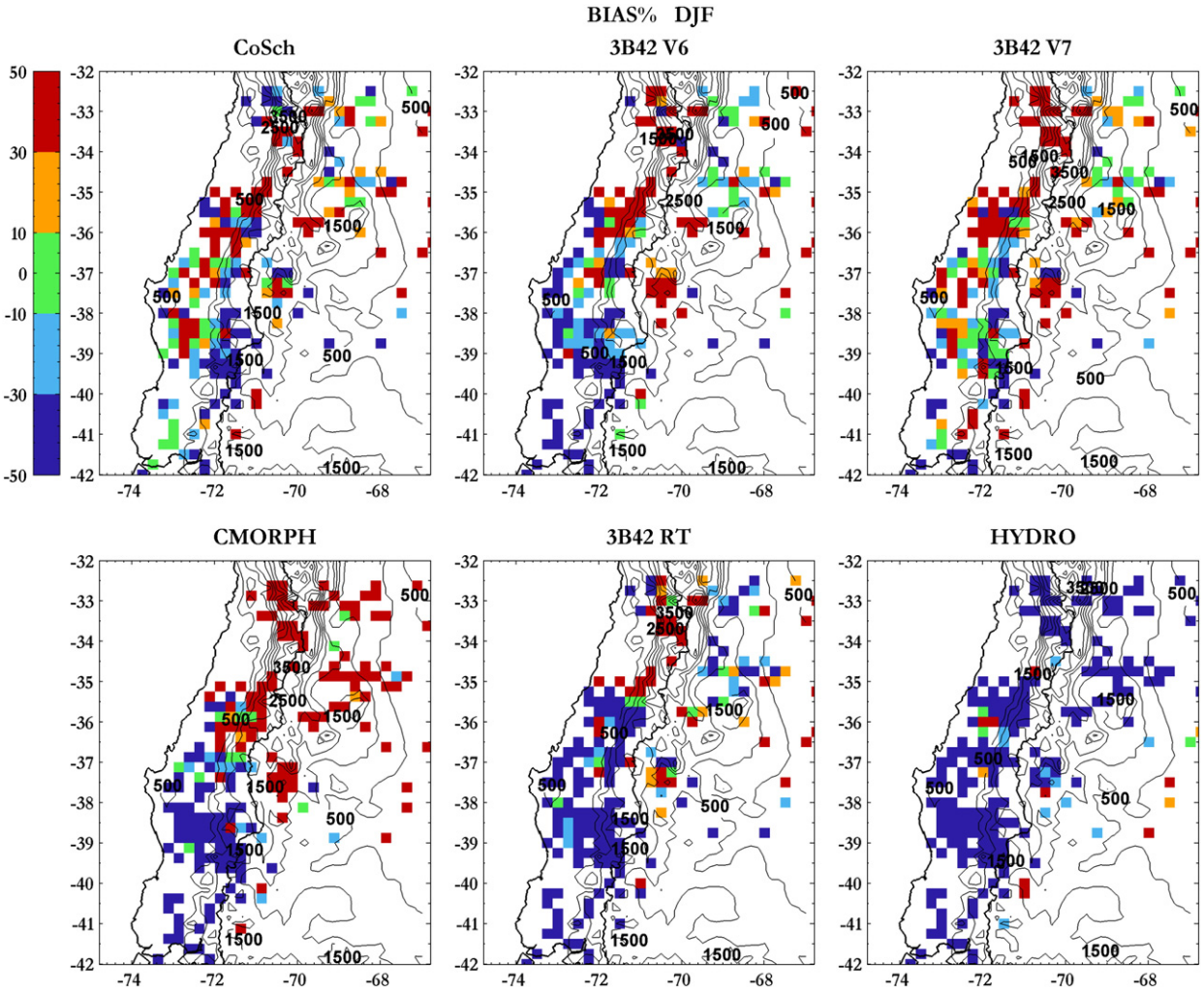

Fig. 6. BIAS% calculated over the Central Andes for austral summer (December–January–February) by the different precipitation estimations considered in the present study.

caused by incoming cold fronts and occasional rain episodes below the freezing level (Garreaud, 2013). The high mountain area has a marked snow regime with an important winter component. Unfortunately, no data are available above 3500 m that allow for observation of this cycle, but operational stations will be installed in the high mountains areas in the coming years. In contrast, leeward of the Andes, precipitation is restricted to summer and is associated with storms (García-Ortega et al., 2009; De la Torre et al., 2004). Estimate performance over this area is low because it is very difficult for algorithms to capture the presence of snow or the warm storms below the freezing level. This poses a major challenge to the development of new algorithms over mountainous areas and may be addressed by future satellite constellations, such as the Global Precipitation Measurement Mission — GPM.

Although CMORPH underestimates precipitation on the annual scale, when precipitation tends to have a convective nature and occurs leeward of the Andes in summer, it fails by overestimating values. The algorithms associated with 3B42 (RT, V6, V7 and CoSch) present accurate results for the area leeward of the Andes in summer, and the performance of the algorithms that include surface stations is better. In winter, 3B42 V7 tends to underestimate precipitation in areas close to the coast and overestimate precipitation in the high mountains. This behavior is notable between 32° S and 35° S, which evidence the modifications introduced to the algorithm in this version. For different regions of the world, research has been conducted to evaluate rainfall satellite estimates in mountainous regions. The complex terrain represents an additional challenge for estimates and results in the worst performances in these regions (Dinku et al., 2007, 2010a, 2010b; Hirpa et al., 2010; Habib et al., 2012).

3.2. Statistical analysis by region

As mentioned previously, the performance of precipitation estimates varies across regions and seasons. Therefore, statistics – which depend on the number of precipitation events, their genesis and intensity – were calculated for the regions described in Section 2. In general, the precipitation rate over South America is greater during the warm seasons, summer (DJF) and spring (SON). In the area located south of 40° S and in Central Chile, winter is the rainy season (JJA) and estimates generally underestimate the amount of rainfall that occurs during those months. Autumn (MAM) is a transition season in all of the selected areas.

Fig. 8 shows the NRMSE and BIAS% in box SA considering the different seasons. The performance of the estimates depends on the season, which indicates the need for considering the different

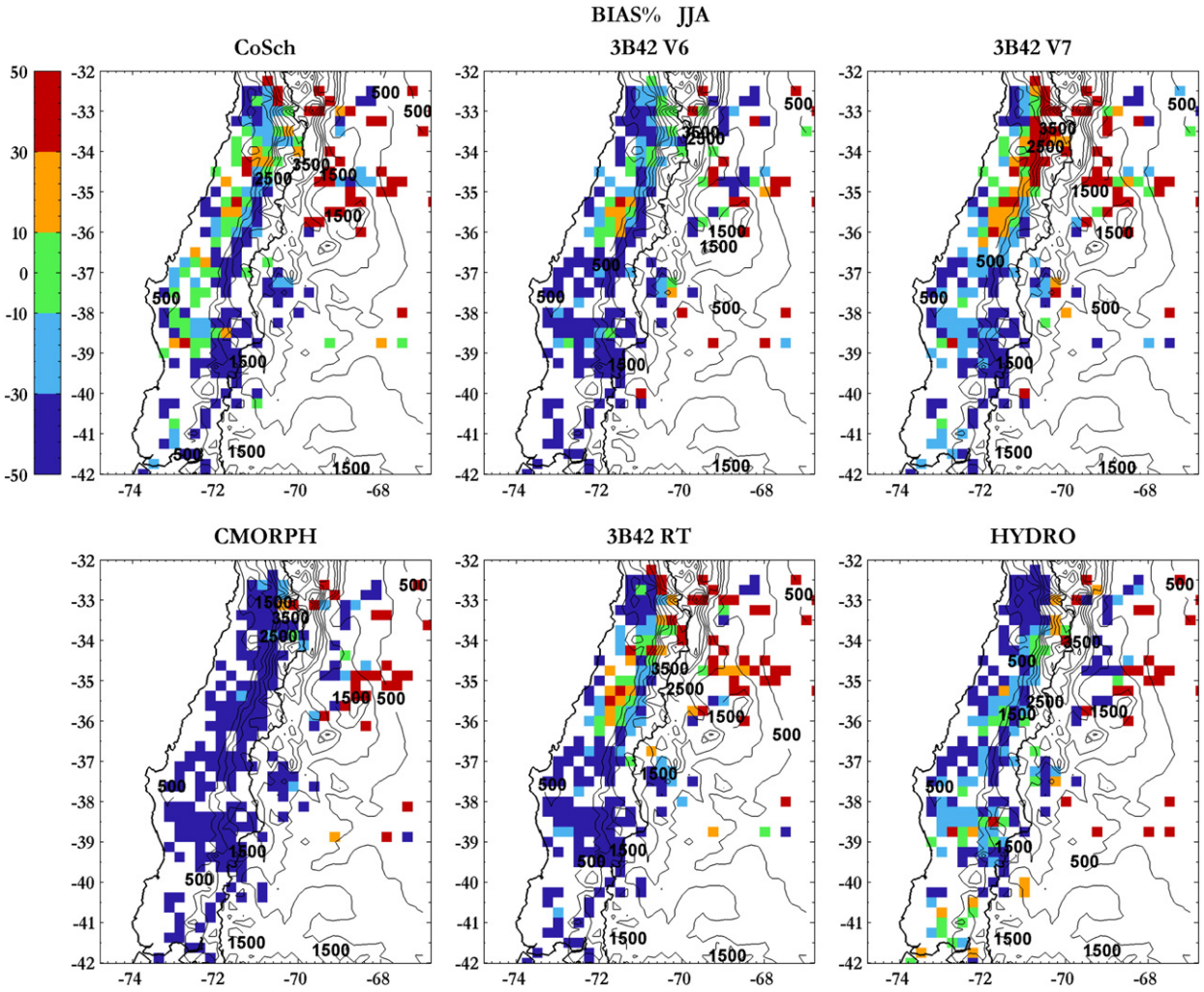

Fig. 7. BIAS% calculated over the Central Andes for austral winter (June–July–August) by the different precipitation estimations considered in the present study.

precipitation regimes when performing the analysis. Region SA shows an increase in the errors in the season with less precipitation. The BIAS% of estimates of CoSch, 3B42 V6, 3B42 V7, 3B42 RT and CMORPH shows an overestimation of precipitation; extreme BIAS% corresponds to CMORPH, which is in agreement with previous results, although estimates have negative bias in winter. On the other hand, the bias of HYDRO is negative throughout the year. Estimations associated with IR data, which is HYDRO in the present study, show a persistent negative bias for the total precipitation over the area and may be due to the method's reliance on cloud top temperatures. In the current version, all cloud systems with temperatures above 241 K have no associated rain, while some stratiform rainfall in this region is associated with higher cloud top temperatures. On the other hand, the maximum rainfall value is also capped at 35 mm/h for heavy rain systems (i.e., MCSs). These limitations produce underestimations all year.

Fig. 9 shows the box plots for BIAS% in the study period in region SA. The analysis of the mean values reveals that 3B42 V6, V7 and RT estimates, as well as CMORPH, produce positive values when the entire time interval is considered; CMORPH and RT yield higher overestimates of precipitation, which are in agreement with previous results. In turn, CoSch produces the best precipitation estimates in the region with a BIAS% closer to zero, a symmetrical distribution and low dispersion; in addition, the absolute values of the atypical values are not as large, unlike CMORPH. In HYDRO estimates, both the mean and the median indicate that this method underestimates rainfall over SA; in addition, the distribution of extremes is biased towards negative values. On the other hand, scattering and extreme values (i.e., distinct differences) are smaller in 3B42 V7 than in RT.

Focusing on the results obtained for the entire study period and the SA region, Fig. 10 assesses the quality of precipitation estimates based on the BIASS, ETS, POD and FAR indices as a function of the selected thresholds. In this region, the BIASS is greater than one at low thresholds for all of the estimates, except HYDRO, and indicates that they overestimate weak precipitation events. Then, for moderate precipitation events – thresholds of 5–20 mm – the bias of all estimates is close to one, while HYDRO underestimates precipitation to a larger degree with an increasing precipitation threshold. Lastly, at high thresholds, both CMORPH and all of the versions of 3B42 considerably overestimate precipitation. CoSch achieves a better performance at all thresholds after the correction with surface observations is introduced, as described above. Notably, of the operational precipitation estimates available (3B42 RT, CMORPH and HYDRO), 3B42 RT provides a better result for this index, which is a measure of systematic errors of the estimates.

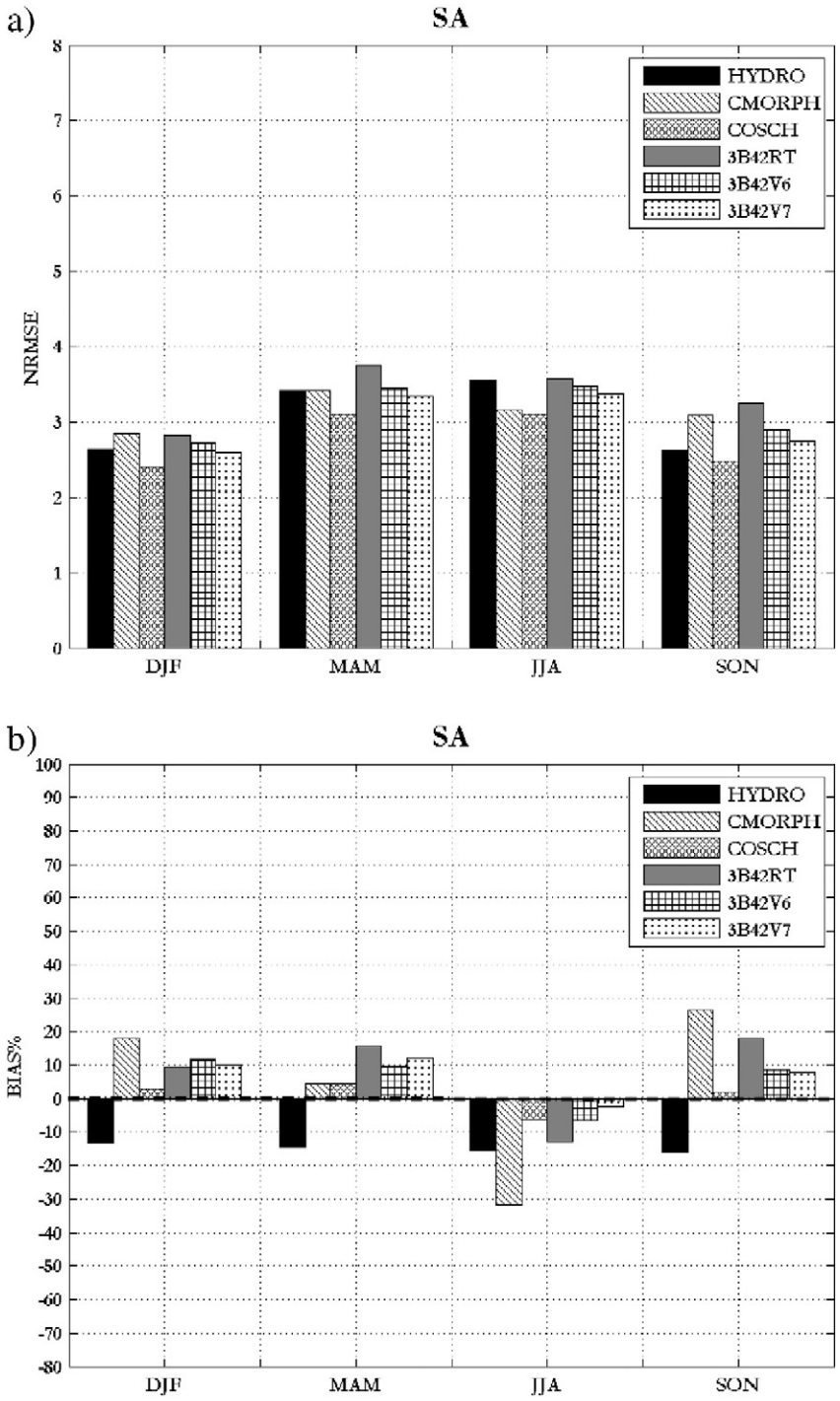

Fig. 8. a) Normalized root mean square error and b) BIAS% calculated for the different seasons in southern South America (SA). DJF stands for December, January and February, MAM is March, April and May, JJA is June, July and August and SON is September, October and November.

The analysis of ETS adds sensitivity to errors associated with the location and the timing of precipitation systems considering the random chance of success. Again, CoSch performs better relative to the other estimates, mainly at low thresholds, and reaches a value slightly higher than 0.4 for the 2 mm threshold. The spatial and temporal performances of estimates worsen with increasing thresholds and indicate the limitations in the accuracy of estimates of extreme precipitation events. In turn, the worst result associated with this index is produced by HYDRO, and the remaining estimates have similar intermediate behaviors.

Again, the POD and FAR indices (Fig. 10c and d, respectively) show that CoSch is more capable of detecting precipitation over the study region. CoSch also presents a low proportion of false alarms compared with other estimates. HYDRO performs the worst with a decreased quality in precipitating system detection and no marked difference in false alarms. The strong dependence of the estimate ability on the precipitation threshold is evident. For instance, in the case of CoSch, the detection probability decreases from approximately 80% for low thresholds to almost 40% for thresholds above 30 mm. In agreement, the false alarm ratio increases with higher thresholds. An interesting

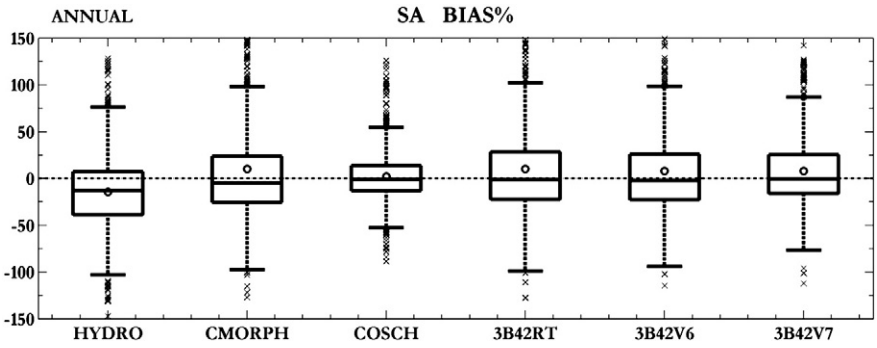

Fig. 9. Boxplot of BIAS% calculated for the different seasons over southern South America (SA). The circles show the mean over all grid points in the region obtained from daily accumulations. Each box represents the 25th and 75th percentiles of the BIAS%, and the lines in the middle of the box represent the median value (50th percentile). The "whiskers" extend to the farthest outlying values that are no more than 1.5 times the interquartile range (difference between the 75th and 25th percentiles) away from the upper or lower limit of the box. The crosses beyond the whiskers denote observed BIAS% values falling farther than 1.5 times the interquartile range from the upper or lower limit of the box.

result is that CMORPH seems to perform better than 3B42 estimates at low thresholds if only the POD index is analyzed. However, when considering the results of the BIASS index, it is evident that although it detects the precipitating systems, the amount of rain that is attributed to them is incorrect. Consequently, several indices providing combined information need to be examined to achieve an adequate verification.

To extend the result in the climatic areas, the PDFs were calculated over the study period (Fig. 11). These probability functions indicate the percentage of precipitation contributed to the total by each of the precipitation thresholds and make it possible to understand which threshold contributes the most to the total precipitation in each region. Moreover, Table 1 includes the ratio between the total estimated accumulated precipitation in the study period and the total observed accumulated precipitation. A ratio greater than 1 indicates that observations are overestimated; when it is below 1, underestimates are produced. In NE, SB and CE, there is clear overestimation by all versions of 3B42 and CMORPH at thresholds above 70 mm, while thresholds between 10 and 70 mm are underestimated. Similar results were found by Demaria et al. (2011); using an object-based verification method, they revealed the existence of systematic errors in 3B42 V6 and CMORPH during MCSs events over the SB region.

On the other hand, the curves obtained from HYDRO and CoSch are similar to the observations at all thresholds, although the analysis of total precipitation in Table 1 reveals that HYDRO clearly underestimates precipitation over the entire area, as shown previously.

The regime in CA is characterized by the presence of windward precipitation, mainly snow, in Chile and in the high mountains in winter. In summer, precipitation occurs mainly on the Argentinean side where severe storms are able to produce precipitation and large hail (Sanchez et al., 2011). All estimates tend to overestimate small values and underestimate large values, except for those of HYDRO whose behavior is opposite. All values underestimate the total precipitation to a large degree in this region; CMORPH yields the largest underestimations. Although these results show trends of the estimates in areas of complex topography, a deeper understanding of the structure of precipitation over these areas, the conditions that favor precipitation development and the type of precipitation (solid or liquid) according to the season is needed. The values in Table 1 show that CA is the area where changes introduced in 3B42 V7 had the greatest impact; although it underestimates the total precipitation, the behavior is better than that of V6 and RT.

Figs. 12 and 13 show the NRMSE and BIAS%, respectively, for the different regions, similarly to Fig. 8 for SA. The NRMSE is always greater in the season when the lowest precipitation rate is recorded. As mentioned, SB and NE are highly affected by MCSs that mainly occur in SON and DJF, a characteristic feature of the precipitation regime. In winter, much less precipitation occurs, which is generally associated with the presence of frontal systems with less convective development (Siqueira and Toledo Machado, 2004). Unfortunately, observational networks are very scarce on the eastern slope of the Andes in northern Argentina and southern Bolivia. Despite being a region of high interest in terms of the onset of convective systems (Romatschke and Houze, 2013), it has not been studied separately due to the lack of observations. The precipitation regimes in NE and SB present very similar characteristics, although the winter dry season is more pronounced in NE. SB, which has the highest precipitation rates, i.e., daily rates above 3 mm in all seasons, has the smallest error estimates. The error in SB CoSch estimates decreases markedly given the great number of observations used for adjusting the estimate. Although in most cases CoSch yields the best results, the error decrease is not as important in the other regions. The analysis of the BIAS reveals that all estimates perform better in SB. In NE, all of the estimates overestimate precipitation, except HYDRO, which has negative BIAS in all seasons. This shows that the estimates based on parameters associated with IR underestimate precipitation; inclusion of microwave data improves the ability to capture convective precipitation, although it generates large overestimations, as seen with CMORPH.

Fig. 14 shows the BIAS% box plots for the different regions in South America. The box plots for NE and SB show strongly contrasting results, although the mean BIAS% indicates that precipitation is overestimated in both cases. Overestimation is much larger in NE than in SB, mainly by those estimates that were not calibrated with surface values (3B42 RT, CMORPH and HYDRO). However, the median is near zero for almost all cases in both regions. CoSch provides smaller extreme values in SB, which is the area with the largest number of observations. CA presents large errors, primarily in summer when precipitation is convective, but large errors can be observed due to the presence of snow on the surface of high mountains. Precipitation is underestimated throughout the year in the region, as was shown in the previous section. Again, the 3B42 V7 BIAS% box plots reveal a reduction in the error dispersion. Although progress has been made in characterizing estimates in the Central Andes – an area of complex topography – more precipitation observations are needed at altitudes above 3500 m to validate the results.

In summer, the CE region may be affected by the onset of MCSs and smaller spatial scale convection (Salio et al., 2007); however, in winter, the region is strongly affected by frontal systems. The increase in the error for winter is remarkable and is related to cold tops associated with cold fronts that produce low precipitation, while in the warm season, the error decreases. Again, HYDRO underestimates precipitation, while the rest of the estimates tend to overestimate precipitation. The BIAS% boxplot shows that 3B42 V7 is able to reduce the interquartile range compared with the other estimates, although the tendency for overestimation persists.

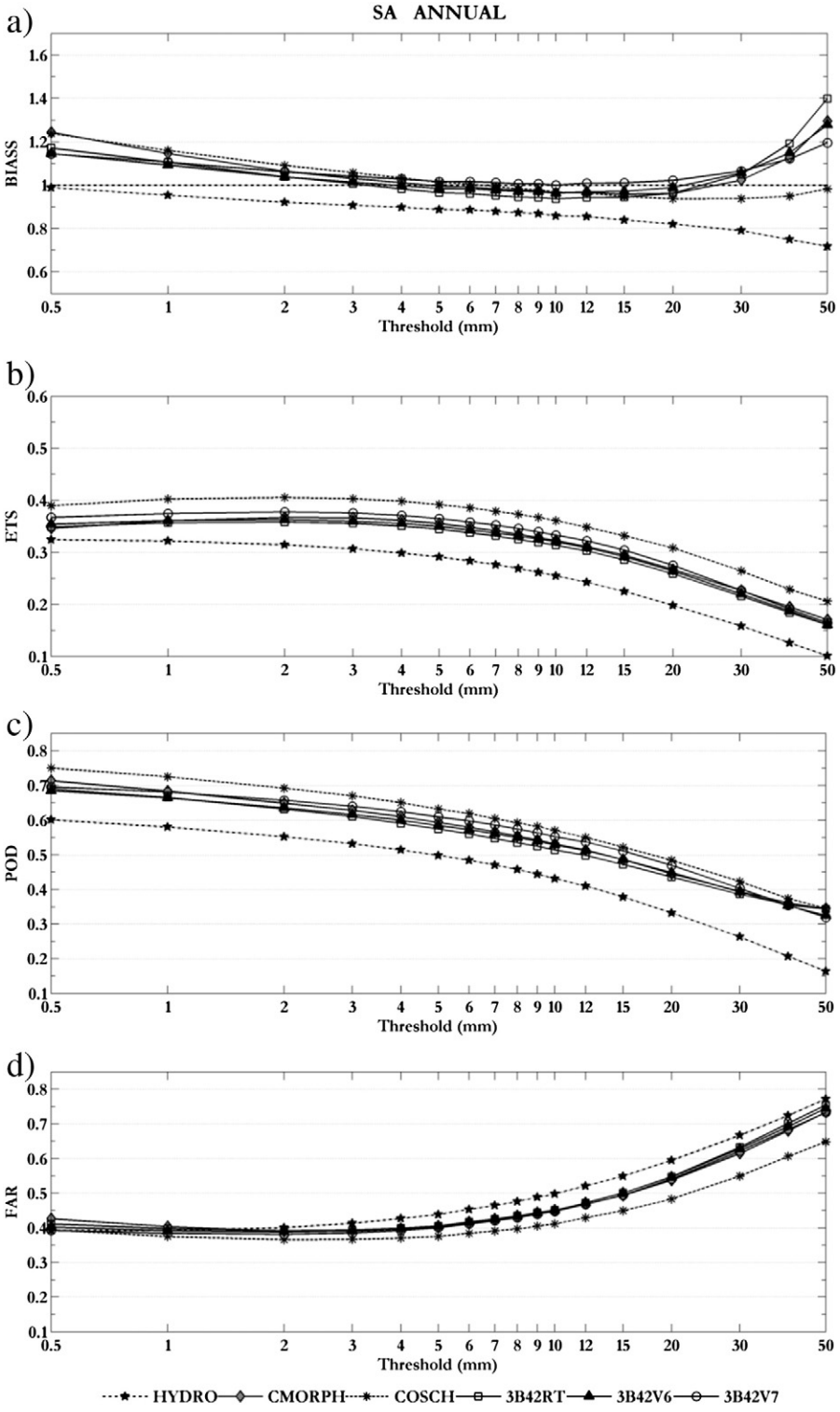

Fig. 10. a) Bias score, b) equitable threat score, c) probability of detection and d) false alarm ratio for the different precipitation estimations over southern South America.

4. Conclusions

Estimates of precipitation derived from remote sensors provide crucial information in areas where observational networks are sparse and irregular; these estimates are very useful for numerous users. Although this study advances the assessment of such estimates, more ground observations undoubtedly are needed to establish an appropriate rain gauge network in South America for time scales shorter than 24 hours. Regional integration of existing networks in South American countries, as well as inter-institutional information exchange, needs to be fostered to deliver real-time products to users. Developing and expanding a network of hourly observations in the region is a priority given the scarcity of operational radars. Progress is also needed in the region in the realization of intensive observation field experiments, such as those conducted under the Global Precipitation Measurement Mission — Ground Validation. The CHUVA experiments developed in various places in Brazil are an example of these types of field experiments (Machado et al., 2014).

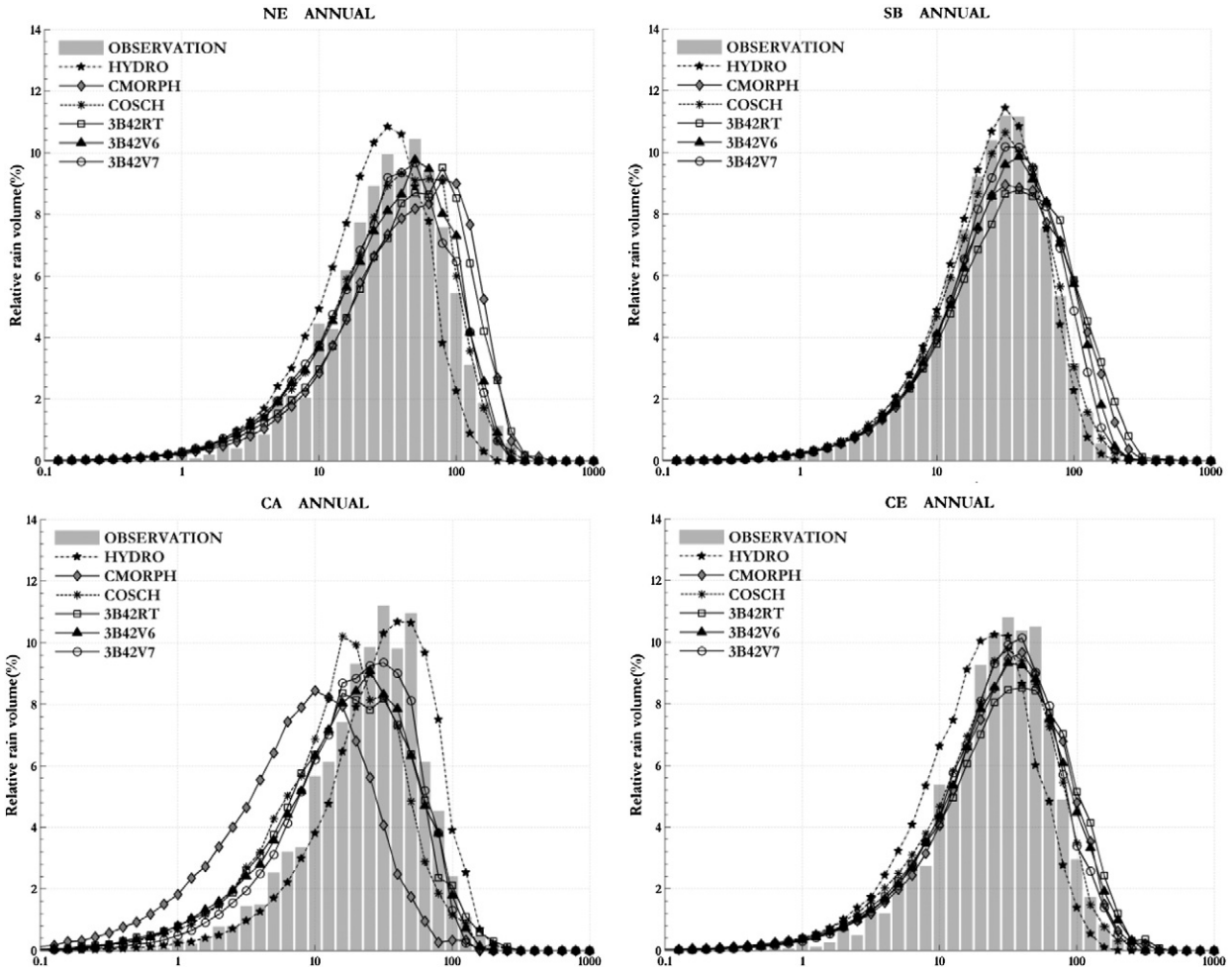

Fig. 11. Distribution of rain volume probability for northeastern Argentina (NE, upper left panel), southern Brazil (SB, upper right panel), Central Andes (CA, lower left panel) and Central Argentina and Uruguay (CE, lower right panel).

The results analyzed in the present study indicate that the performance of precipitation estimate products that include microwave information is remarkable. The performance improves further by including surface observations in the adjustments, as in 3B42 V6, V7 and CoSch. However, a deeper assessment is necessary, particularly regarding the effects of topography and solid-precipitation areas, in view of the persistence of major overestimations of precipitation. Statistical results over regions that are strongly affected by convective systems, such as northern Argentina and southern Brazil, still show a tendency to overestimate precipitation, principally for extreme values higher than 70 mm. Blended techniques perform better for convective regimes around the globe, but mesoscale convective systems in South America are associated with large stratiform and convective areas that produce a significant amount of precipitation; in these cases, overestimates occur. Further research must be performed over the area to determine the origin of these differences.

HYDRO, which is associated with IR data, shows a persistent negative bias for total precipitation, possibly because this methodology relies on cloud top temperatures. In the current version, all cloud systems with temperatures above 241 K have no associated rain, while some stratiform rainfall in this region is associated with higher cloud top temperatures. On the other hand, the maximum rainfall value is also capped at 35 mm/h for heavy rain systems. These limitations produce underestimations all year.

These results show the importance of integrated multi-satellite products that could combine MW and IR retrievals, tracking algorithms and surface observation calibrations to provide real-time products to different users in the area. Future work should focus on different regimes that generate precipitation (warm or convective regimes) to fully understand the discrepancies between the estimates and to provide more insight into the physical reasons why measurements differ.

Table 1
Total volumetric precipitation accumulated during the entire study period in each selected region. Numbers in parentheses represent the ratio between total estimated precipitation and total observed precipitation. NE: northeastern Argentina, CE: Central Argentina and Uruguay, CA: Central Andes (CA) and SB: southern Brazil.

	Pixels	Obs	CoSch	CMORPH	HYDRO	3B42 RT	3B42 V6	3B42 V7
NE	241	344 509	422 241 (1.23)	579 441 (1.68)	300 401 (0.87)	480 696 (1.40)	425 194 (1.23)	422 649 (1.23)
SB	766	2 151 295	2 195 848 (1.02)	2 459 468 (1.14)	1 906 844 (0.89)	2 382 971 (1.11)	2 351 075 (1.09)	2 346 715 (1.09)
CA	244	400 685	256 505 (0.64)	151 360 (0.38)	249 649 (0.62)	205 778 (0.51)	207 909 (0.52)	297 007 (0.74)
CE	522	726 841	910 221 (1.25)	1 062 695 (1.46)	617 761 (0.85)	1 019 338 (1.40)	926 732 (1.28)	869 842 (1.20)

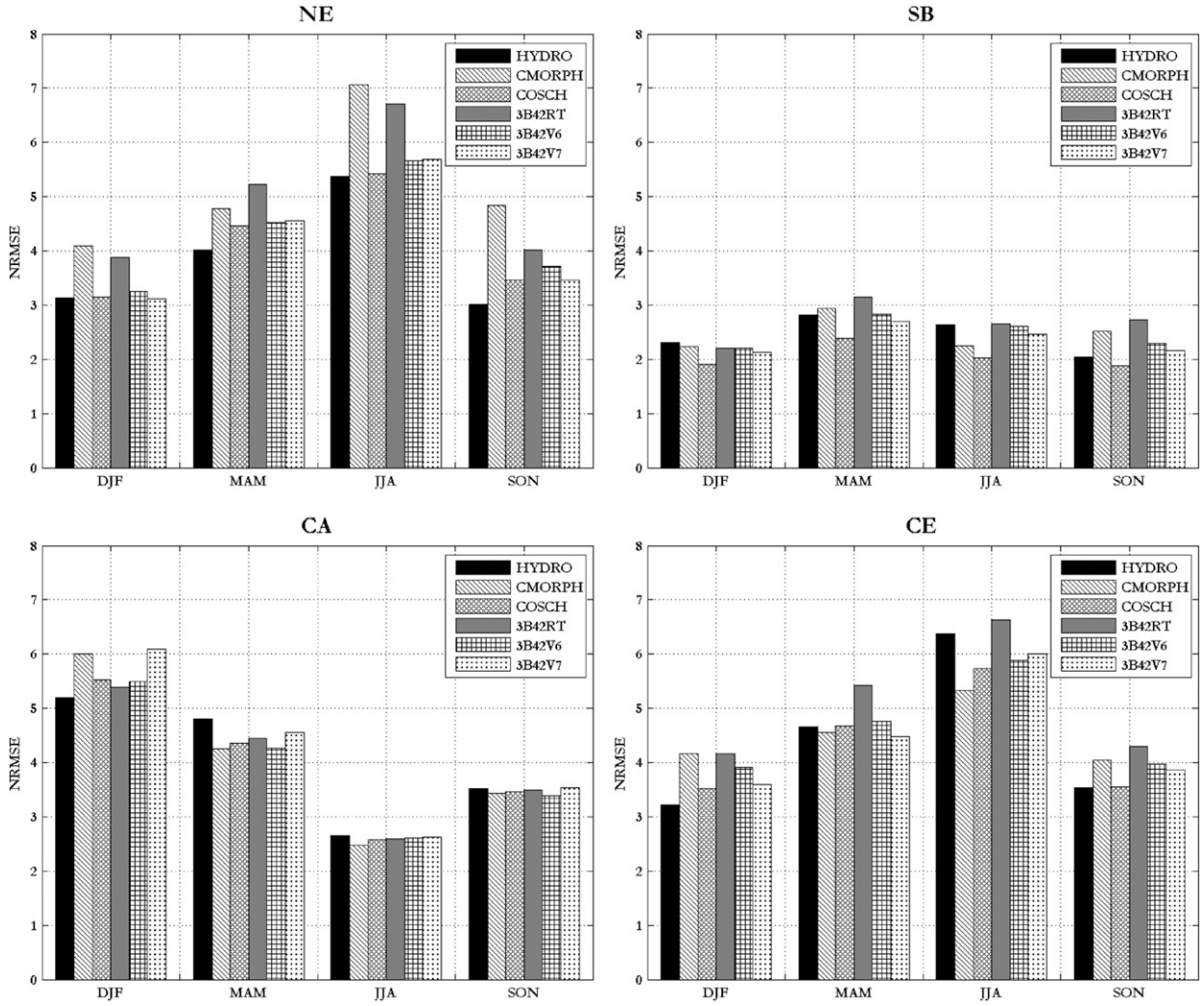

Fig. 12. Normalized root mean square error calculated for the different seasons in southern South America. The regions considered are northeastern Argentina (NE, upper left panel), southern Brazil (SB, upper right panel), Central Andes (CA, lower left panel) and Central Argentina and Uruguay (CE, lower right panel). DJF stands for December, January and February, MAM is March, April and May, JJA is June, July and August and SON is September, October and November.

Acknowledgments

This work was funded by ANPCyT PICT 2008-215, ANPCyT PICT 2007-355, CNRS LEFE: averses sud-américaines, CONICET-CNPQ 2699/12, and CONICET-NICET 490394/2011-6. We are deeply grateful to three anonymous reviewers who helped us to improve the article and provide their insightful comments. We would like to acknowledge the cooperation from David Allured, Mario Bidegain, Daniel Cielak, Federico Claus, Rene Garreaud, Brant Liebmann, Cynthia Matsudo, and Gabriela Migale for providing rain gauge data for the present study.

References

Amitai, E., Petersen, W., Llort, X., Vasiloff, S., 2012. Multiplatform comparisons of rain intensity for extreme precipitation events. IEEE Trans. Geosci. Remote Sens. 50 (3), 675–686. http://dx.doi.org/10.1109/TGRS.2011.2162737.

Arkin, Phillip A., Meisner, Bernard N., 1987. The relationship between large-scale convective rainfall and cold cloud over the western hemisphere during 1982–84. Mon. Weather Rev. 115, 51–74. http://dx.doi.org/10.1175/1520-0493(1987)115<0051:TRBLSC>2.0.CO;2.

De la Torre, A., Daniel, V., Tailleux, R., Teitelbaum, H., 2004. A deep convection event above the tunuyán valley near the Andes Mountains. Mon. Weather Rev. 132, 2259–2268. http://dx.doi.org/10.1175/1520-0493(2004)132<2259:ADCEAT>2.0.CO;2.

De Vera, Alejandra, Terra, Rafael, 2012. Combining CMORPH and rain gauges observations over the Rio Negro Basin. J. Hydrometeorol. 13, 1799–1809. http://dx.doi.org/10.1175/JHM-D-12-010.1.

Demaria, E.M.C., Rodriguez, D.A., Ebert, E.E., Salio, P., Su, F., Valdes, J.B., 2011. Evaluation of mesoscale convective systems in South America using multiple satellite products and an object-based approach. J. Geophys. Res. 116, D08103. http://dx.doi.org/10.1029/2010JD015157.

Dinku, T., Ceccato, P., Grover-Kopec, E., Lemma, M., Connor, S.J., Ropelewski, C.F., 2007. Validation of satellite rainfall products over East Africa's complex topography. Int. J. Remote Sens. 28 (7), 1503–1526.

Dinku, T., Connor, S.J., Ceccato, P., 2010a. Comparison of CMORPH and TRMM-3B42 over mountainous regions of Africa and South America. Satellite Rainfall Applications for Surface Hydrology, pp. 193–204.

Dinku, T., Ruiz, F., Connor, S.J., Ceccato, P., 2010b. Validation and intercomparison of satellite rainfall estimates over Colombia. J. Appl. Meteorol. Climatol. 49 (5), 1004–1014.

Ebert, E.E., Manton, M.J., Arkin, P.A., Allam, R.J., Holpin, G.E., Gruber, A.J., 1996. Results from the GPCP Algorithm Intercomparison Programme. Bull. Am. Meteorol. Soc. 77, 2875–2887.

Ebert, Elizabeth E., Janowiak, John E., Kidd, Chris, 2007. Comparison of near-real-time precipitation estimates from satellite observations and numerical models. Bull. Am. Meteorol. Soc. 88, 47–64. http://dx.doi.org/10.1175/BAMS-88-1-47.

García-Ortega, E., López, L., Sánchez, J.L., 2009. Diagnosis and sensitivity study of two severe storm events in the Southeastern Andes. Atmos. Res. 93 (1–3), 161–178.

Garreaud, R., 2013. Warm winter storms in central Chile. J. Hydrometeorol. 14, 1515–1534. http://dx.doi.org/10.1175/JHM-D-12-0135.1.

Gochis, D.J., Nesbitt, S.W., Yu, W., Williams, S., 2009. Comparison of gauge-corrected versus non-gauge corrected satellite-based quantitative precipitation estimates during the 2004 NAME Enhanced Observing period. Atmosfera 22, 69–98.

Habib, E., El Saadani, M., Haile, A.T., 2012. Climatology-focused evaluation of CMORPH and TMPA satellite rainfall products over the Nile Basin. J. Appl. Meteorol. Climatol. 51 (12), 2105–2121.

Hirpa, F.A., Gebremichael, M., Hopson, T., 2010. Evaluation of high-resolution satellite precipitation products over very complex terrain in Ethiopia. J. Appl. Meteorol. Climatol. 49 (5), 1044–1051.

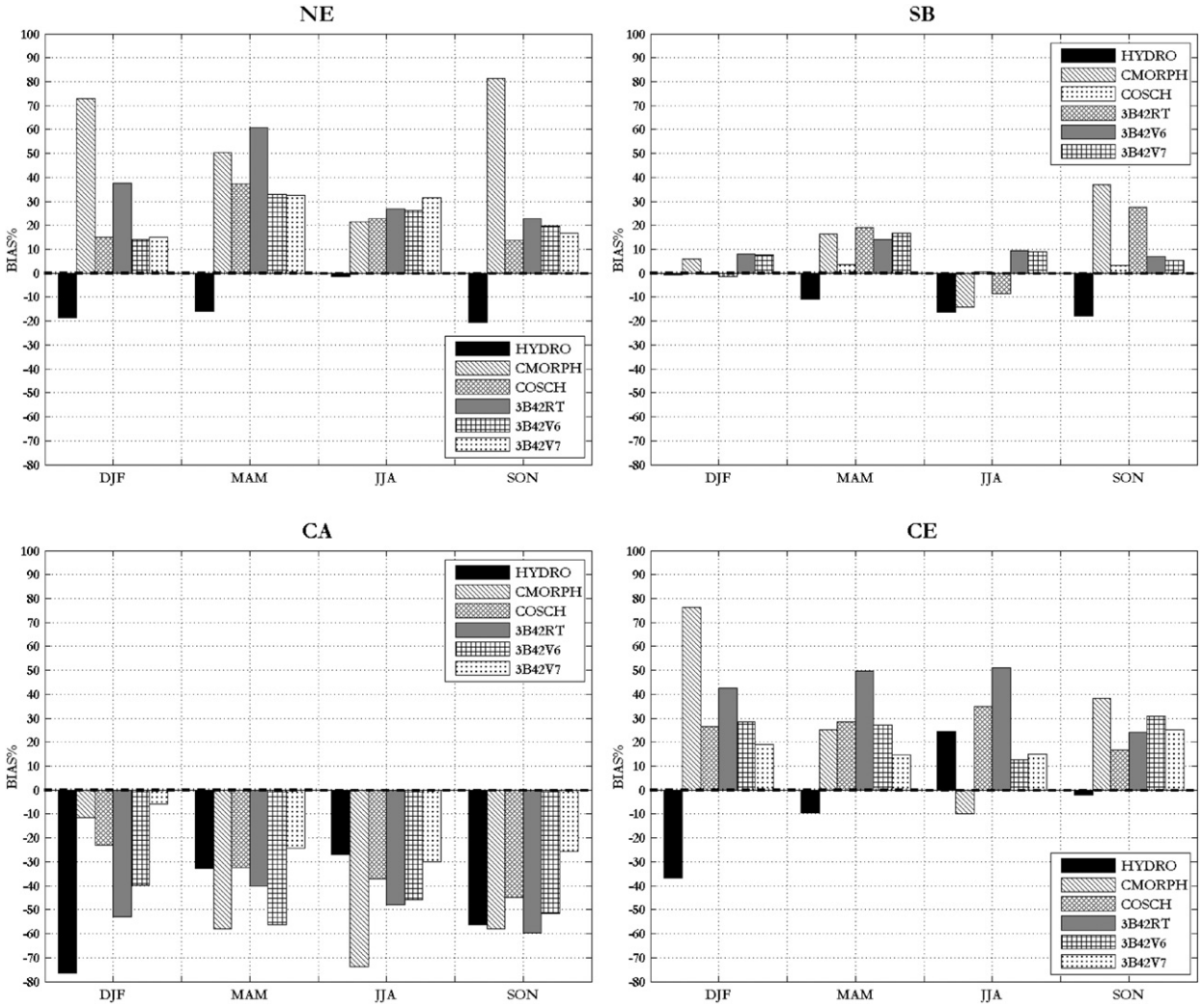

Fig. 13. The same as in Fig. 12 but for BIAS%.

Houze, R.A., 1994. Cloud Dinamics. Academic Press (573 pp.).

Huffman, G.J., Bolvin, D.T., 2013. TRMM and Other Data Precipitation Data Set Documentation, Lab. for Atmos., NASA Goddard Space Flight Cent. and Sci. Syst. and Appl. Available at:. http://precip.gsfc.nasa.gov/pub/trmmdocs/3B42_3B43_doc.pdf.

Huffman, George J., Adler, Robert F., Morrissey, Mark M., Bolvin, David T., Curtis, Scott, Joyce, Robert, McGavock, Brad, Susskind, Joel, 2001. Global precipitation at one-degree daily resolution from multisatellite observations. J. Hydrometeorol. 2, 36–50. http://dx.doi.org/10.1175/1525-7541(2001)002<0036:GPAODD>2.0.CO;2.

Huffman, George J., et al., 2007. The TRMM multisatellite precipitation analysis (TMPA): quasi-global, multiyear, combined-sensor precipitation estimates at fine scales. J. Hydrometeorol. 8, 38–55. http://dx.doi.org/10.1175/JHM560.1.

Joyce, Robert J., Janowiak, John E., Arkin, Phillip A., Xie, Pingping, 2004. CMORPH: a method that produces global precipitation estimates from passive microwave and infrared data at high spatial and temporal resolution. J. Hydrometeorol. 5, 487–503. http://dx.doi.org/10.1175/1525-7541(2004)005<0487:CAMTPG>2.0.CO;2.

Kidd, C., Levizzani, V., 2011. Status of satellite precipitation retrievals. Hydrol. Earth Syst. Sci. 15, 1109–1116.

Kidd, C.K., Kniveton, D.R., Todd, M.C., Bellerby, T.J., 2003. Satellite rainfall estimation using combined passive microwave and infrared algorithms. J. Hydrometeorol. 4, 1088–1104.

Kucera, P.A., Ebert, E.E., Turk, F.J., Levizzani, V., Kirschbaum, D., Tapiador, F.J., Loew, A., Borsche, M., 2013. Precipitation from space: advancing earth system science. Bull. Am. Meteorol. Soc. 94, 365–375. http://dx.doi.org/10.1175/BAMS-D-11-00171.1.

Kuligowski, R.J., 2002. A self-calibrating real-time GOES rainfall algorithm for short-term rainfall estimates. J. Hydrometeorol. 3, 112–130. http://dx.doi.org/10.1175/1525-7541(2002)003<0112:ASCRTG>2.0.CO;2.

Liebmann, B., Allured, D., 2005. Daily precipitation grids for South America. Bull. Am. Meteorol. Soc. 86, 1567–1570. http://dx.doi.org/10.1175/BAMS-86-11-1567.

Liu, C., Zipser, E.J., 2009. "Warm Rain" in the tropics: seasonal and regional distributions based on 9 yr of TRMM data. J. Clim. 22, 767–779. http://dx.doi.org/10.1175/2008JCLI2641.1.

Machado, L.A.T., Silva Dias, M.A.F., Morales, C., Fisch, G., Vila, D., Albrecht, R., Goodman, S.J., Calheiros, A.J.P., Biscaro, T., Kummerow, C., Cohen, J., Fitzjarrald, D., Nascimento, E.L., Sakamoto, M.S., Cunningham, C., Chaboureau, J.-P., Petersen, W.A., Adams, D.K., Baldini, L., Angelis, C.F., Sapucci, L.F., Salio, P., Barbosa, H.M.J., Landulfo, E., Souza, R.A.F., Blakeslee, R.J., Bailey, J., Freitas, S., Lima, W.F.A., Tokay, A., 2014. The Chuva Project: How Does Convection Vary across Brazil? Bull. Amer. Meteor. Soc. 95, 1365–1380. http://dx.doi.org/10.1175/BAMS-D-13-00084.1.

Miller, S.W., Arkin, P.A., Joyce, R., 2001. A combined microwave/infrared rain rate algorithm. Int. J. Remote Sens. 22, 3285–3307.

Porcu, F., Milani, L., Petracca, M., 2014. On the uncertainties in validating satellite instantaneous rainfall estimates with raingauge operational network. Atmos. Res. 144, 73–81. http://dx.doi.org/10.1016/j.atmosres.2013.12.007.

Romatschke, U., Houze, R.A., 2013. Characteristics of precipitating convective systems accounting for the summer rainfall of tropical and subtropical South America. J. Hydrometeorol. 14, 25–46. http://dx.doi.org/10.1175/JHM-D-12-060.1.

Rozante, J.R., Soares Moreira, D., de Goncalves, L.G.G., Vila, D.A., 2010. Combining TRMM and surface observations of precipitation: technique and validation over South America. Weather Forecast. 25, 885–894. http://dx.doi.org/10.1175/2010WAF2222325.1.

Ruiz, J.J., 2009. Evaluation of different methodologies to calibrate CMORPH over Sudamerica. Rev. Bras. Meteorol. 24 (4), 473–488 (in spanish).

Salio, P., Nicolini, M., Zipser, E.J., 2007. Mesoscale convective systems over southeastern South America and their relationship with the South American low-level jet. Mon. Weather Rev. 135, 1290–1309. http://dx.doi.org/10.1175/MWR3305.1.

Sanchez, J.L., Gil-Robles, B., Dessens, J., Martin, E., Lopez, L., Marcosa, J.L., Berthetb, C., Fernández, J.T., García-Ortega, E., 2011. Characterization of hailstone size spectra in hailpad networks in France, Spain, and Argentina. Atmos. Res. 93 (1–3), 641–654.

Sapiano, M.R.P., Arkin, P.A., 2009. An intercomparison and validation of high-resolution satellite precipitation estimates with 3-hourly gauge data. J. Hydrometeorol. 10, 149–166. http://dx.doi.org/10.1175/2008JHM1052.1.

Schwerdtfeger, W., 1976. World survey of climatology. Climates of Central and South America vol. 12. Elsevier.

Scofield, R.A., Kuligowski, R.J., 2003. Status and outlook of operational satellite precipitation algorithms for extreme-precipitation events. Weather Forecast. 18, 1037–1051. http://dx.doi.org/10.1175/1520-0434(2003)018<1037:SAOOOS>2.0.CO;2.

Siqueira, J.R., Toledo Machado, L.A., 2004. Influence of the frontal systems on the day-to-day convection variability over South America. J. Clim. 17 (9), 1754–1766.

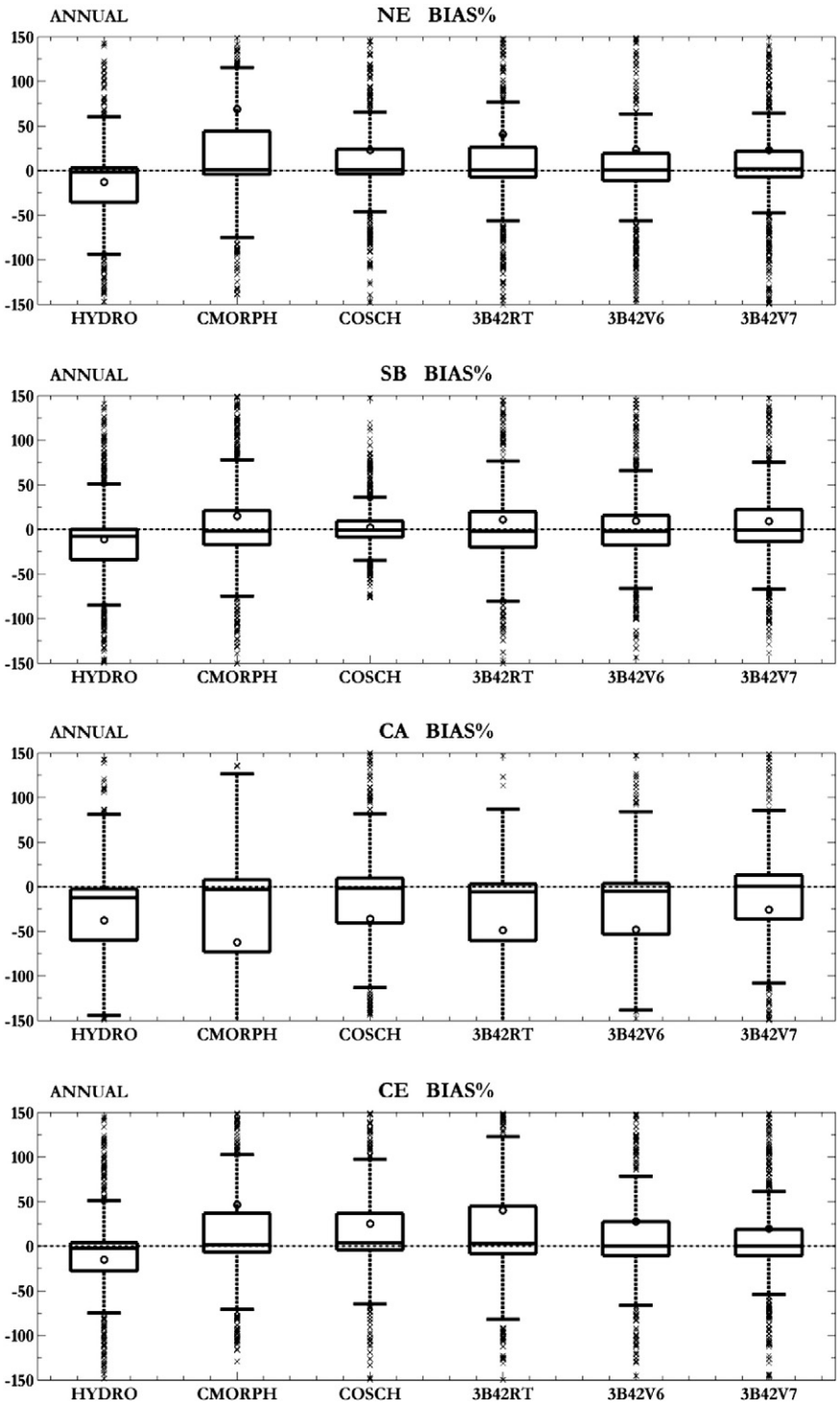

Fig. 14. The same as in Fig. 9 but for northeastern Argentina (NE, top panel), southern Brazil (SB, upper central panel), Central Andes (CA, lower central panel) and Central Argentina and Uruguay (CE, bottom panel).

Smith, E.A., Lamm, J.E., Adler, R.F., Alishouse, J., Aonashi, K., 1998. Results of the WetNet PIP-2 project. J. Atmos. Sci. 55, 1483–1536.

Sorooshian, S., Hsu, Kuo-Lin, Gao, X., Gupta, H.V., Imam, B., Braithwaite, Dan, 2000. Evaluation of PERSIANN system satellite-based estimates of tropical rainfall. Bull. Am. Meteorol. Soc. 81, 2035–2046. http://dx.doi.org/10.1175/1520-0477(2000)081<2035:EOPSSE>2.3.CO;2.

Strahler, A.N., 1969. Physical Geography. 3rd ed. Wiley, New York.

Su, F., Hong, Y., Lettenmaier, D.P., 2008. Evaluation of TRMM Multisatellite Precipitation Analysis (TMPA) and its utility in hydrologic prediction in the La Plata Basin. J. Hydrometeorol. 9 (4), 622–640.

Tapiador, F.J., Turk, F.J., Petersen, W., Hou, A.Y., García-Ortega, E., Machado, L.A.T., Angelis, C.F., Salio, P., Kidd, C., Huffman, G.J., de Castro, M., 2012. Global precipitation measurement: methods, datasets and applications. Atmos. Res. 104–105, 70–97.

Vicente, G., Scofield, R., Davenport, J., 2001. The role of orographic and parallax corrections on real time high resolution satellite rainfall rate distribution. Int. J. Remote Sens. 23 (2), 221–230.

Vila, D.A., Scofield, R., Davenport, J., 2002. Satellite rainfall estimation over South America: evaluation of two major events. AMS 16th Conference on Hydrology, pp. 33–36.

Vila, D.A., de Goncalves, L., Toll, D.L., Rozante, J.R., 2009. Statistical evaluation of combined daily gauge observations and rainfall satellite estimates over continental South America. J. Hydrometeorol. 10, 533–543. http://dx.doi.org/10.1175/2008JHM1048.1.

Xu, L., Gao, X., Sorooshian, S., Arkin, P.A., Imam, B., 1999. A microwave infrared threshold technique to improve the GOES precipitation index. J. Appl. Meteorol. 38, 569–579.

Zipser, E.J., Cecil, D.J., Liu, C., Nesbitt, S.W., Yorty, D.P., 2006. Where are the most intense thunderstorms on Earth? Bull. Am. Meteorol. Soc. 87, 1057–1071.